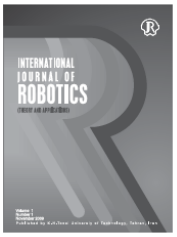

INTERNATIONAL JOURNAL OF ROBOTICS
(THEORY AND APPLICATIONS)
E-mail: IJR@kntu.ac.ir

Stable Gait Planning and Robustness Analysis of a Biped Robot with One Degree of Underactuation

R. Dehghani[a], A. Fattah[b]*

a-Department of Mechanical Engineering, Isfahan University of Technology, Isfahan, 8415683111, Iran, Email: rezadehghani@me.iut.ac.ir
b-Corresponding author, Department of Mechanical Engineering, Isfahan University of Technology, Isfahan, 8415683111, Iran, Email: fattah@cc.iut.ac.ir

ARTICLE INFO

Keywords:
Biped robot
Underactuation
Poincaré map
Robust motion

ABSTRACT

In this paper, stability analysis of walking gaits and robustness analysis are developed for a five-link and four-actuator biped robot. Stability conditions are derived by studying unactuated dynamics and using the Poincaré map associated with periodic walking gaits. A stable gait is designed by an optimization process satisfying physical constraints and stability conditions. Also, considering underactuation problem, a time-invariant control law is designed to track the stable motion of biped. Validation of proposed approach is achieved by numerical simulations. Moreover, the robustness of motion on the uneven surfaces and elastic contact model are investigated.

1. Introduction

The design and motion control of bipedal robots are one of the challenging topics in the field of robotics and are recently considered by a great number of researchers and engineers. Bipedal walking robots can be divided into two broad classes. The first class is fully-actuated bipedal robots. In these bipeds, the control of bipedal walking robots is mostly carried out with methods based on tracking of temporal reference trajectories generally associated with the control of the Zero Moment Point (ZMP) [1,2]. The ZMP stability principal states that the biped will not fall down as long as the ZMP remains inside the hull of the foot-support [3].

The second broad class consists of passive-dynamic walkers and limit-cycle walkers. Inspired by the completely passive walkers of McGeer [4], these robots forgo full actuation and allow gravity and the natural dynamics to play a large part in the generation of motion. They may be completely passive, or partially actuated [5].

To achieve fast walking gaits, investigators are studied a walking mechanism as a compass like biped with point feet [6-8]. However, in this case, the stability criterion ZMP cannot be used and the control problem

and stability analysis become more difficult. Control of walking gaits of these robots is a very interesting and simultaneously difficult problem. Important medical applications of bipeds with point feet include prostheses for the lower limbs and rehabilitation of statics balancing and walking.

For these types, it is possible dynamically to stabilize their specific walking gaits. For instance, the convergence to a nominal cyclic motion is improved in [9], by changing the step length or the trunk orientation. The feedback linearization method is utilized to control the walking cycle during the single support phase for a novel nearly linear model in [10]. In [11], a partial feedback linearization has used to control the entire walking cycle including the single support phase (SSP) and double support phase (DSP). In [12], the existence of the limit cycles is studied for a special class of underactuated bipeds using differential flatness and controlled the biped robot off-line. Using the neural network to have a robust control for this type of bipeds is another method presented in [13]. In [14], the dynamical stability of a three-link biped is presented under a control law being finite time convergent. In [15] it is shown that it is possible to track in single support stable trajectories with internal stability by a suitable choice of outputs for a two-link robot and for a five-link robot. The Hybrid Zero Dynamics (HZD) has developed for planar biped walkers with a torso and one degree of underactuation in [16]. Controller has been designed based on the judicious choice of a set

of holonomic constraints that were asymptotically imposed on the robot via feedback control. This was accomplished by interpreting the constraints as output functions in which the number of constraints are equal to the number of inputs and then combining with computed torque method for control motion. However, in this method the motion converges to cyclic motion after several gaits (for instance 15 gaits in [17]) since the output constraints are only followed. In [18], using the sliding mode control only for the generalized coordinates of the lower body, a stable motion for upper body have resulted such that the robot converges to cyclic motion after 160 steps.

In most of previous works, the biped motion converges to a cyclic motion after several gaits as presented in [17,18]. However, in this research work, an approach is proposed such that the biped converges to the cyclic motion with faster convergence. For instance, we will show in the simulation results the biped converges to cyclic motion after four gaits.

In this paper, a five-link biped robot with point feet is investigated. For this robot, there is no actuator at contact point foot and hence it is considered as one degree of underactuation system. As a result, it cannot track any arbitrary path and we define the joint trajectories parameterized in terms of a time-scale function. The stability conditions of periodic orbits are then derived by analyzing the stability of unactuated dynamic model. Using minimization of mechanical work during motion, subjected to physical constraints and stability conditions, desired joint space trajectories are obtained. Furthermore, a time-invariant control law is developed in order to track the stable motion. Several simulations are accomplished to show efficiency of this approach. Also, robustness of motion on the uneven surface and a compliant model of walking surface are studied.

The rest of paper is organized as follows. The dynamical model of the robot at hand and its equations of motion are presented in Section 2. In Section 3, we present a discussion of stability and optimization problem in order to design the stable gait. Motion control strategy and resolving underactuation problem are described in Section 4. Simulation results are presented in Section 5. In Section 6, we study robustness of motion on the uneven surfaces. The flexible contact model is presented in Section 7 and its simulation results are shown. Conclusions are presented in Section 8.

2. Modeling

The dynamic model of a biped robot with five links is shown in Fig. 1. It consists of a torso, two hips, and two identical legs where each leg articulated by a knee and without feet. The model assumes point feet with no actuation between the stance leg and the ground and full actuation at all other joints. Walking is taken place in the sagittal plane (the plane that divides the body into left and right halves).

The stability in the frontal plane can be achieved with only frontal plane control actions [19]. Motion involved the single support phase where only the stance leg is on the ground and the impact phase where the swing leg hits on the ground. These two phases of the walking cycle naturally lead to the differential equations describing the dynamics during the single support phase and a discrete model of the dynamics of the impact phase.

2.1. Single Support Phase Model

In the single support phase, the end of the stance leg is acting as a pivot and thus there are five degrees of freedom. The angular coordinates of the shanks, thighs and torso are indicated in Fig. 1. Identical model is used for both legs and thus the legs are switched after each impact. The dynamic model during single support phase between two successive impacts can be derived using the Lagrange method. The equations of motion in the single support phase can be written as

$$\begin{aligned} &\mathbf{M}(\mathbf{q})\ddot{\mathbf{q}} + \mathbf{C}(\mathbf{q},\dot{\mathbf{q}})\dot{\mathbf{q}} + \mathbf{g}(\mathbf{q}) = \mathbf{B}\boldsymbol{\tau} \\ &\mathbf{q} = [\theta_1, \theta_2, \theta_3, \theta_4, \theta_5]^T, \boldsymbol{\tau} = [\tau_{k_1}, \tau_H, \tau_{k_2}, \tau_T]^T \end{aligned} \quad (1)$$

Here, $\mathbf{M}(\mathbf{q}) \in R^{5\times5}$ is the mass matrix and $\mathbf{C}(\mathbf{q},\dot{\mathbf{q}}) \in R^{5\times5}$ contains Coriolis and centrifugal forces. Also, $\mathbf{g}(\mathbf{q}) \in R^5$ is the gravity force vector and $\mathbf{B} \in \mathrm{R}^{5\times4}$ is a constant matrix for torque distribution. Two actuators are provided at hips and denoted by τ_H and τ_T also two actuators at the knee joints denoted by τ_{k_1} and τ_{k_2}. There is no any actuator at the end of legs. Hence, the number of actuators is less than the degrees of freedom and thus the robot is underactuated by one and matrix B has one column less than its row. This causes the dynamic model (1) is divided into unactuated and actuated dynamics. Their expressions are

$$\begin{aligned} &\overline{\mathbf{M}}(\mathbf{q})\ddot{\mathbf{q}} + \overline{\mathbf{C}}(\mathbf{q},\dot{\mathbf{q}})\dot{\mathbf{q}} + \overline{g}(\mathbf{q}) = 0 \\ &\overline{\overline{\mathbf{M}}}(\mathbf{q})\ddot{\mathbf{q}} + \overline{\overline{\mathbf{C}}}(\mathbf{q},\dot{\mathbf{q}})\dot{\mathbf{q}} + \overline{\overline{\mathbf{g}}}(\mathbf{q}) = \boldsymbol{\tau} \end{aligned} \quad (2)$$

where

$$\overline{\mathbf{M}} = \mathbf{B}^{\perp}\mathbf{M}, \quad \overline{\mathbf{C}} = \mathbf{B}^{\perp}\mathbf{C}, \quad \overline{g} = \mathbf{B}^{\perp}\mathbf{g}$$
$$\overline{\overline{\mathbf{M}}} = \mathbf{B}^{+}\mathbf{M}, \quad \overline{\overline{\mathbf{C}}} = \mathbf{B}^{+}\mathbf{C}, \quad \overline{\overline{\mathbf{g}}} = \mathbf{B}^{+}\mathbf{g}$$

Here, $\mathbf{B}^{\perp} \in \mathrm{R}^{1\times5}$ and $\mathbf{B}^{+} \in \mathrm{R}^{4\times5}$ are orthogonal complement and pseudo-inverse matrices of B, respectively, i.e., $\mathbf{B}^{\perp}\mathbf{B} = \mathbf{0}, \mathbf{B}^{+}\mathbf{B} = \mathbf{I}_{4\times4}$. The orthogonal complement $\mathbf{B}^{\perp}$ can be chosen as $\mathbf{B}^{\perp} = [b_c, \mathbf{0}_{1\times4}]$ where bc is a non-zero constant. Also, the pseudo-inverse $\mathbf{B}^{+}$ can be given as $\mathbf{B}^{+} = (\mathbf{B}^T\mathbf{B})^{-1}\mathbf{B}^T$.

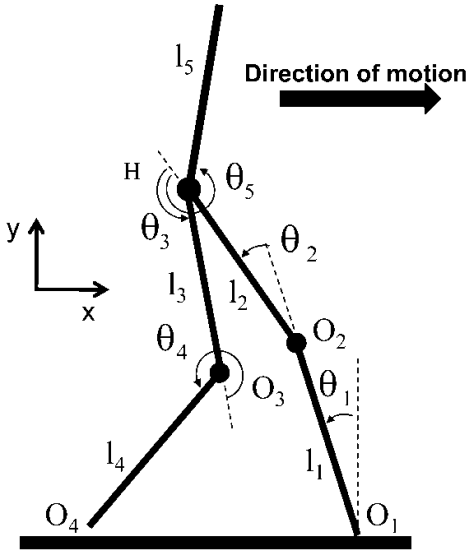

Fig. 1: Schematic of a five-link biped robot in sagittal plane

Remark 1. It may be noted that the kinetic energy of the robot is independent of the choice of world coordinate frame and thus it is independent of θ_1 because the joint angle θ_1 only fixes the world coordinate frame.

2.2. Impact Model

At the end of the single support phase, the heel of the swing leg hits on the ground while the stance leg leaves the ground. On applying the principle of the angular impulse and momentum for a system of n bodies connected by revolute joints, one can determine the joint velocities after the impact in terms of the joint velocities before the impact [20]. In addition to modeling the change in state of the robot, the impact model accounts for the relabeling of the robot coordinates that occurs after each impact. The following hypotheses are used for the impact model.

H1) Impact is considered as a plastic contact such that velocity of impact point is zero after hitting.

H2) Joint angles before and after the impact remain the same while the angular velocities change instantaneously.

H3) Impact is instantaneous and the stance leg lifts from the ground without interaction at the moment of impact.

These assumptions imply total angular momentum is conserved [20]. Using the principle of the angular impulse and momentum, we express the velocity of the robot just after impact in terms the velocity just before impact without relabeling.

In order to derive the angular velocity of links after impact, we consider five subsystems as follows

SS1: Right leg, i.e., O1-O2.

SS2: Right leg and right thigh, i.e., O1-O2-H.

SS3: Right leg, right thigh and torso.

SS4: Right leg, right thigh, torso, left thigh.

SS5: The whole system.

Now, we use the conservation of angular momentum for the five subsystems of the biped robot at impact moment as

$$\mathbf{H}^{+}_{O_2} = \mathbf{H}^{-}_{O_2}, \quad \mathbf{H}^{+}_{2H} = \mathbf{H}^{-}_{2H}, \quad \mathbf{H}^{+}_{3H} = \mathbf{H}^{-}_{3H}$$
$$\mathbf{H}^{+}_{O_3} = \mathbf{H}^{-}_{O_3}, \quad \mathbf{H}^{+}_{O_4} = \mathbf{H}^{-}_{O_4} \tag{3}$$

Here, $\mathbf{H}_{o_2}$ is the total angular momentum of subsystem SS1 about O_2 and $\mathbf{H}_{2H}$ is the total angular momentum of subsystem SS2 about H. Also, $\mathbf{H}_{3H}$, $\mathbf{H}_{O_3}$ and $\mathbf{H}_{O_4}$ are the total angular momentum of subsystem SS3, SS4 and SS5 about H, O_3 and O_4, respectively.

Using (3), the joint rates after impact for the biped robot are given in terms of the joint rates before the impact as

$$\dot{\mathbf{q}}^{+} = \mathbf{\Delta}_{\mathbf{q}}(\mathbf{q})\dot{\mathbf{q}}^{-} \tag{4}$$

After impact, it is assumed that the swing leg becomes the new stance leg, so the coordinates must be relabeled. We can express the relabeling of the states as a linear, invertible transformation matrix E.

The result of the impact and relabeling of the rates for the kth gait is then given as:

$$\dot{\mathbf{q}}^{+}_{k+1} = \mathbf{E}\mathbf{\Delta}_{\mathbf{q}}(\mathbf{q}^{-}_{k})\dot{\mathbf{q}}^{-}_{k} \tag{5}$$

The joint angles do not change during the impact phase, so they are given after impact by permutation matrix in terms of the joint angles before impact as

$$\mathbf{q}^{+}_{k+1} = \mathbf{E}\mathbf{q}^{-}_{k} + \mathbf{d} \tag{6}$$

where d is a constant vector. Hence, the (k+1)th gait begins by the initial states (5) and (6).

3. Gait Planning

The problem of gait planning for biped robots is fundamentally different from the path planning for traditional fixed base manipulator arms. For gait planning of the biped robot with point feet, one has to consider stability condition during motion. The ZMP criterion cannot be used for this biped because of the point feet. Also, this robot cannot follow any arbitrary trajectory due to the underactuation problem and may fall on the ground for an arbitrary trajectory. In this section, a stability analysis is presented and then the gait planning is described for this underactuated biped robot.

3.1. Stability Analysis

As mentioned in pervious section this biped is an underactuated system and the dynamics of system is divided into actuated and unactuated dynamics such that only actuated dynamic can be controlled using actuators. In this section, we obtain conditions to guarantee stable motion for this biped robot. To this end, we derive conditions that lead to make unactuated dynamics stable during motion.

The first equation of (2) shows unactuated dynamics during single support phase.

Theorem 1: If we define $\zeta = \mathbf{B}^{\perp}\mathbf{M}\dot{\mathbf{q}}$, the equation of unactuated dynamics during the single support phase can be written as

$$\dot{\zeta} = -\phi_1(\mathbf{q}) \tag{7}$$

Proof: Having $\zeta = \mathbf{B}^{\perp}\mathbf{M}\dot{\mathbf{q}}$, the time derivative of ζ is written as follows

$$\dot{\zeta} = \mathbf{B}^{\perp}\mathbf{M}\ddot{\mathbf{q}} + \mathbf{B}^{\perp}\dot{\mathbf{M}}\dot{\mathbf{q}} \tag{8}$$

Due to the fact that kinetic energy is not a function of θ_1 and the form of $\mathbf{B}^{\perp}$, we can deduce $\overline{\mathbf{C}} = \mathbf{B}^{\perp}\dot{\mathbf{M}}\dot{\mathbf{q}}$. Hence, the equation of unactuated dynamics (i.e., first equation of (2)) is rewritten as

$$\dot{\zeta} + \mathbf{B}^{\perp}\mathbf{g}(\mathbf{q}) = 0 \tag{9}$$

Therefore, we obtain (7) if we define $\phi_1(\mathbf{q}) = \mathbf{B}^{\perp}\mathbf{g}(\mathbf{q})$. If the generalized coordinates are given in terms of time trajectories and having $\zeta(t) \neq 0$ during motion, we can multiply (7) by scalar ζ and integrate the result thus obtained with respect to time to obtain $\zeta(t)$ as

$$\zeta^2 = \zeta_0^2 - 2\int_0^t \left(\phi_1(\mathbf{q}(t))\left[\mathbf{B}^{\perp}\mathbf{M}(\mathbf{q}(t))\dot{\mathbf{q}}(t)\right]\right) dt \tag{10}$$

where, ζ_0 is initial value of ζ.

However, since there is not any actuator at o_1, the period of a half of gait cycle is unknown and thus one cannot obtain a time trajectory for all joints. Therefore, the right hand side of (10) cannot be evaluated and thus $\zeta(t)$ cannot be determined from (10). To overcome this problem, we express the generalized coordinates in terms of a time-scale parameter s as $\mathbf{q}(t) = \mathbf{q}(s(t))$ in which $s(t)$ is a monotonic function and changes between 0 and 1 such that the gait is started at $s = 0$ and the swing leg hits on the ground at $s = 1$.

On the other hand, the initial value of ζ after kth gait is evaluated by the impact equation (5) as

$$\begin{aligned}\zeta_{k+1}^{+} &= \mathbf{B}^{\perp}\mathbf{M}(\mathbf{q}_{k+1}^{+})\dot{\mathbf{q}}_{k+1}^{+} \\ &= \mathbf{B}^{\perp}\mathbf{M}(\mathbf{q}_{k+1}^{+})\mathbf{E}\Delta_{\dot{\mathbf{q}}}(\mathbf{q}_k^{-})\dot{\mathbf{q}}_k^{-}\end{aligned} \tag{11}$$

Upon substitution of the time-scale trajectories into (11), we can rewrite (11) as

$$\zeta_{k+1}^{+} = \Delta_{\zeta}\zeta_k^{-} \tag{12}$$

with

$$\Delta_{\zeta} = \frac{\mathbf{B}^{\perp}\mathbf{M}(\mathbf{q}_{k+1}^{+})\mathbf{E}\Delta_{\dot{q}}(\mathbf{q}_k^{-})\mathbf{q}_k'(1)}{\mathbf{B}^{\perp}\mathbf{M}(\mathbf{q}_k^{-})\mathbf{q}_k'(1)}$$

Here, $\mathbf{q}' = \dfrac{d\mathbf{q}(s)}{ds}$. Now we study the stability motion of the unactuated dynamic, i.e., (7), during motion. To this end, we consider (7) and (12) for the (k+1)th gait as the single support phase and impact phase, respectively and use the parameterized trajectories for the generalized coordinates.

The complete model of unactuated dynamic during motion at (k+1)th gait are given by using (7) and (12) as

$$\begin{cases}\dot{\zeta}_{k+1} = -\phi_1(\mathbf{q}) & \mathbf{q}^{-} \notin S \\ \zeta_0 = \Delta_{\zeta}\zeta_1 & \mathbf{q}^{-} \in S\end{cases} \tag{13}$$

Here, $\zeta_1 = \zeta_k(s=1)$, $\zeta_0 = \zeta_{k+1}(s=0)$ and $S = \left\{\mathbf{q} \middle| y_{o_4}(\mathbf{q}) = 0, x_{o_4}(\mathbf{q}) > 0\right\}$ is the hyper plane in which the impact occurs (see Fig. 1). On the other hand, because there is no actuator at O_1, thus the biped can walk forward while the sign of the total angular momentum of system about O_1 does not change during forward motion. We can obtain the total angular momentum of system about O_1 by dividing ζ by bc.

Therefore, the forward motion of this biped is guaranteed by $\zeta = \mathbf{B}^{\perp}\mathbf{M}\mathbf{q}'\dot{\mathbf{s}} \neq 0$ during single support phase. Now, we choose bc as a positive number and since $\mathbf{s}(t)$ is an increasing function ($\dot{s}(t)$ is positive for forward motion), we can obtain a forward motion condition as follows

$$\mathbf{B}^{\perp}\mathbf{M}\mathbf{q}'(\mathrm{s}) < 0 \quad 0 \le s \le 1 \tag{14}$$

In the following, we study stability of dynamic model (13) by considering (14) during periodic motion. An important tool to analyze the stability of periodic orbit is Poincaré map where it replaces a continuous nth-order time system by a discrete (n-1)th-order time system [21]. Here in this research work, Poincaré map method is used to analyze the stability of the biped motion during periodic gaits.

Since $\zeta(s) \neq 0$, we can multiply the first equation of (13) by scalar ζ and integrate the result thus obtained with respect to s parameter. Hence, we write (10) in terms of time-scale s and then integrate with respect to s to get

$$\zeta_{k+1}^2(s) = \zeta_0^2 - \phi_2(s) \tag{15}$$

where ,

$$\phi_2(s) = 2\int_0^s \left(\phi_1(\eta)\left[\mathbf{B}^{\perp}\mathbf{M}(\eta)\mathbf{q}'(\eta)\right]\right) \mathrm{d}\eta.$$

Moreover, value ζ at the end of the single support phase should be more than its initial value at the beginning of this phase because of the kinetic energy loss during impact. This implies that $\phi_2(s=1) < 0$ to compensate the kinetic energy loss due to impact phase.

Remark 2: The biped robot can complete a gait planned as function of time-scale parameter s, if and only if we have $\zeta_0^2 - \max_{0\le s\le 1}(\phi_2(s)) > 0$.

The effect of the impact is also added into (15) by substituting ζ_0^2 from the second equation of (13) as

$$\zeta_{k+1}^2(s) = \Delta_{\zeta}^2\zeta_1^2 - \phi_2(s) \tag{16}$$

Since the left hand side of (16) is a positive quantity, the right hand side of this equation should be also a positive quantity. On the other word, the following condition should be satisfy

$$\Delta_{\zeta}^2\zeta_1^2 - \max_{0\le s\le 1}(\phi_2(s)) > 0 \tag{17}$$

A walking motion is a periodic orbit during different phases. The Poincaré return map is an appropriate mathematical tool in order to analyze the stability of periodic orbits. Here, we intend to obtain a Poincaré map p such that it maps the impact surface in kth gait into the impact surface in (k+1)th gait, i.e., $p: S_k \to S_{k+1}$. Stability conditions are determined by stability analysis of the fixed points of this map.

Theorem 2: Let the unactuted dynamics be in terms

of the variable ζ as defined in (13) during motion. Then Poincaré returns map of the unactuated dynamics $p: S_k \to S_{k+1}$ is defined by

$$p(\eta_k) = \Delta_\zeta^2 \eta_k - \phi_2(1) \tag{18}$$

and the domain of definition for this map is given by

$$D_p = \{\eta_k \mid \Delta_\zeta^2 \eta_k - \max_{0\le s\le 1}(\phi_2(s)) > 0\} \tag{19}$$

Proof: The unactuated dynamics (13) may be integrated over (k+1)th step and the reinitialization rule (the second equation of (13)) can be applied, the result thus is given as described in (16). Now, we choose the generalized coordinates in $s = 1$ for Poincaré section S and rewrite equation (16) for this moment as

$$\eta_{k+1} = \Delta_\zeta^2 \eta_k - \phi_2(1) \tag{20}$$

where $\eta = \zeta^2(s=1)$. Then, Poincaré map p is obtained from (20) such that $S_k \to S_{k+1}$ as given in (18). Also, using (17), the domain of definition for this map is obtained as (19).

The fixed points of this map should be studied for its stability analysis, A point $\eta^* \in D_p$ is said to be a fixed point of p if $p(\eta^*) = \eta^*$. Hence, the fixed point of p is given by (18) as

$$\eta^* = \frac{\phi_2(1)}{\Delta_\zeta^2 - 1} \tag{21}$$

$\eta^* \in D_p$ is an asymptotically stable equilibrium point of $\eta_{k+1} = p(\eta_k)$ if and only if the eigenvalues of $D_\eta p(\eta^*)$, the Jacobian linearization of p at η^*, have magnitude strictly less than one. Therefore, $\Delta_\zeta^2 < 1$ guaranties stability of Poincaré map p.

Having $\Delta_\zeta^2 < 1$ and η^* in the domain of definition with the fact that $\phi_2(1) < 0$, one can deduce that η^* is an asymptotically stable fixed point for map $p(\eta_k) = \eta_{k+1}$ with domain D_p. In other words, above discussion leads to the following corollary.

Corollary 1: There is a periodic gait in terms of time-scale s, if the following conditions are satisfied.

$$\Delta_\zeta^2 < 1 \quad , \frac{\Delta_\zeta^2 \phi_2(1)}{\Delta_\zeta^2 - 1} - \max_{0\le s\le 1}(\phi_2(s)) > 0 \tag{22}$$

Note that the second part of (22) is derived by substituting (21) into (19).

Thereby, we derived conditions (22) to guarantee the stable motion of unactuated dynamics during the single support and the impact phases based on Poincaré map. More precisely, if (22) can be held for a set of generalized coordinates, $\mathbf{q}(s)$, then the unactuated dynamics is stable during motion.

The aforementioned stability analysis has not accounted for the allowed friction cone at the support leg end. Therefore, we will add no slipping and no lifting of the stance leg constraints on the stability conditions.

The tangential and normal reaction forces at the heel of the stance leg during single support phase are given, respectively, by

$$\begin{aligned} F_t &= m_t \ddot{x}_G = F_t(\mathbf{q}, \dot{\mathbf{q}}, \ddot{\mathbf{q}}) \\ F_n &= m_t(g + \ddot{y}_G) = F_n(\mathbf{q}, \dot{\mathbf{q}}, \ddot{\mathbf{q}}) \end{aligned} \tag{23}$$

where m_t is the total mass of biped and g is the gravitational acceleration, also $\ddot{x}_G$ and $\ddot{y}_G$ are the horizontal and vertical accelerations of the center of mass of whole system, respectively. The relations for these accelerations can be determined by the second time derivative of

$$x_G(\mathbf{q}) = \frac{1}{m_t}\sum_{i=1}^{5} m_i \bar{x}_i(\mathbf{q}), \quad y_G(\mathbf{q}) = \frac{1}{m_t}\sum_{i=1}^{5} m_i \bar{y}_i(\mathbf{q}) \tag{24}$$

where $\bar{x}_i(\mathbf{q})$ and $\bar{y}_i(\mathbf{q})$ are the horizontal and vertical components of the center of mass of link i, respectively. Now, we assume that the biped robot follows the parameterized trajectories. Therefore, using chain rule formula, $\dot{\mathbf{q}}(t)$ and $\ddot{\mathbf{q}}(t)$ are given in terms of parameter s by

$$\begin{aligned} \dot{\mathbf{q}} &= \mathbf{q}'(s)\dot{s} \\ \ddot{\mathbf{q}} &= \mathbf{q}''(s)\dot{s}^2 + \mathbf{q}'(s)\ddot{s} \end{aligned} \tag{25}$$

Moreover, $\dot{s}^2$ and $\ddot{s}$ are obtained by substituting (25) into (16) and the first equation of motion described in (2), as

$$\dot{s}^2(s) = \frac{1}{\left(\overline{\mathbf{M}}\mathbf{q}'(s)\right)^2}\left[\Delta_\zeta^2 \eta_k - \phi_2(s)\right] \tag{26}$$

$$\ddot{s}(s) = \frac{1}{\overline{\mathbf{M}}\mathbf{q}'(s)}\left[-\overline{\mathbf{C}}(s,\dot{s})\mathbf{q}'(s)\dot{s} - \overline{g}(\mathbf{q}(s)) - \overline{\mathbf{M}}\mathbf{q}''(s)\dot{s}^2\right] \tag{27}$$

Substituting (25)-(27) into (23), one can derive the heel reaction forces of the stance leg as

$$\begin{aligned} F_t = F_t(s) = m_t &\left[\sum_{i=1}^{5}\sum_{j=1}^{5}\frac{\partial^2 x_G}{\partial q_i \partial q_j} q_i' q_j' + \sum_{i=1}^{5}\frac{\partial x_G}{\partial q_i} q_i''\right]\dot{s}^2 \\ &+ m_t \sum_{i=1}^{5}\frac{\partial x_G}{\partial q_i} q_i' \ddot{s} \end{aligned} \tag{28}$$

$$\begin{aligned} F_n = F_n(s) = m_t &\left[\sum_{i=1}^{5}\sum_{j=1}^{5}\frac{\partial^2 y_G}{\partial q_i \partial q_j} q_i' q_j' + \sum_{i=1}^{5}\frac{\partial y_G}{\partial q_i} q_i''\right]\dot{s}^2 \\ &- m_t\left[\sum_{i=1}^{5}\frac{\partial y_G}{\partial q_i} q_i'\ddot{s} - g\right] \end{aligned} \tag{29}$$

The force of friction should be enough to prevent slipping. Therefore, necessary conditions to prevent lifting and slipping are given based on the law of Coulomb friction respectively as

$$\begin{cases} F_n(s) > 0 \\ \left|F_t(s)\right| < \mu_s F_n(s) \end{cases} \quad 0 \le s \le 1 \tag{30}$$

where μ_s is the static coefficient of friction between the foot and the ground.

The domain of Poincaré return map p is modified by including no slipping and no bouncing conditions (30) into (19) as

$$D_p = \left\{\eta_k \left| \Delta_\zeta^2 \eta_k - \max_{0\le s\le 1}(\phi_2(s)) > 0, \min_{0\le s\le 1} F_n(s) > 0, \max_{0\le s\le 1}\left(\frac{|F_t(s)|}{F_n(s)}\right) < \mu_s \right.\right\} \tag{31}$$

Therefore, the stability conditions of the unactuated dynamics (7) were obtained by Poincaré map method. In the next subsection, the gait planning of the biped is determined by imposing these stability conditions.

3.2. Stable motion planning with optimization

The previous subsection has provided the conditions for the existence of a periodic motion for the dynamics model with impacts and established its stability properties. In this subsection, we generate a reference motion in the joint space for biped by using optimization and enforcing stability conditions.

It is assumed that the joint angles during the single support phase are known at the intermediate and at the end of the phase. Also, here only symmetric gaits are of interest and the identical model is used for the first and second half of a gait cycle with the coordinates relabeled. For symmetric gait, initial joint angles are determined by swapping legs at the end of the single support phase as $\mathbf{q}(0) = \mathbf{E}\mathbf{q}(1) + \mathbf{d}$. Also, the initial and final joint angle rates are related together by impact equations (5).

The goal of the optimization will be to minimize an appropriate cost function while simultaneously satisfying a number of constraints. In order to generate an efficient gait, we use mechanical work applied during one half of gait cycle as a cost function to be minimized using the following index

$$J = \int_{0^+}^{T} \left|\dot{\mathbf{q}}^T \mathbf{B}\boldsymbol{\tau}\right| dt = \int_0^1 \left|\mathbf{q}'^T \mathbf{B}\boldsymbol{\tau}\right| ds \qquad (32)$$

Here, T is the period of a half gait cycle. The joint torques are given by substituting desired trajectories, defined in terms of time-scale parameter, into the second equation of (2) as

$$\boldsymbol{\tau} = \overline{\overline{\mathbf{M}}}(\mathbf{q})[\mathbf{q}'_d(s)\ddot{s} + \mathbf{q}''(s)\dot{s}^2] + \overline{\overline{\mathbf{C}}}(\mathbf{q},\mathbf{q}'\dot{s})\mathbf{q}'\dot{s} + \overline{\overline{\mathbf{g}}}(\mathbf{q}) \qquad (33)$$

where $\dot{s}^2$ and $\ddot{s}$ have been already defined in (26) and (27).

In order to design a stable gait, we use the stability conditions described in previous subsection for desired trajectories.

By considering above descriptions, the optimization problem for generation of the stable motion is summarized as follows

(i) In order to satisfy the constraints, we select the following fifth-order polynomial functions for each joint trajectory in term of time-scale parameter s

$$q_{di}(s) = a_{5i}s^5 + a_{4i}s^4 + a_{3i}s^3 + a_{2i}s^2 + a_{1i}s + a_{0i} \quad 1 \le i \le 5 \qquad (34)$$

Here, q_{di} is the desired trajectory of ith joint.

Coefficients of these polynomials a_{ij} and the initial slope of time-scale parameter ($\dot{s}_0$) are unknown and determined during optimization.

(ii) By choosing the position of the hip point and the heel of the swing leg at $s = 1$ and $s = 1/2$, we solve the inverse kinematic equations for lower body and determine the joint positions of each leg at initial and intermediate of step. In order to save space, the inverse kinematics equations have been eliminated. Also, the desired posture of torso is chosen upright at $s = 1$ and $s = 1/2$.

(iii) The cost function J is minimized under constraints divided into three classes a) Boundary equality constraints; Constraints on the joint angles at the intermediate and end of single support phase, i.e., q(s=1/2) and q(s=1). The impact equations for angular position and velocities, i.e., $\mathbf{q}(0) = \mathbf{E}\mathbf{q}(1) + \mathbf{d}$ and $\mathbf{q}'(s=0)\dot{s}_0 = \mathbf{E}\boldsymbol{\Delta}_{\mathbf{q}}(\mathbf{q}(s=1))\mathbf{q}'(s=1)\dot{s}_1$ where $\dot{s}_1$ can be obtained using (26) at s=1.

b) Nonlinear inequality constraints; The forward motion constraint (14).No slipping and no bouncing conditions (30).

The boundary of motion of the knees flexion (stance and swing legs), i.e., $0 < q_2 < \pi$ and $-\pi < q_4 < 0$.

No contact between the swing leg and ground during single support phase.

c) Stability constraints;

Stability conditions and existence cyclic motion described in subsection 3.1, i.e., (22) and considering domain of Poincaré map(31).

Remark 3. As the optimization constraints are satisfied for motion planning, we ensure that this reference motion is stable during different phases since the stability of the unactuated dynamics has been satisfied for this stable gait generation.

4. Control Design

In previous Section, the periodic desired trajectories (34) were expressed in terms of the time-scale parameter s. In order to have a stable motion, controller should track the time-scale trajectories during the single support phase before the impact happens. Now, we propose a time-invariant feedback to track time scaled trajectories during motion. Controller has to bring the swing leg at the desired position to hit on the ground in a finite time.

Suppose that a desired trajectory $\mathbf{q}_d(s(t))$ has been designed for the stable motion, according to the discussion in Section 3. To ensure trajectory tracking by the joint variable, the angular position error e of the joints from desired paths are defined as $\mathbf{e} = \mathbf{q}_d(s(t)) - \mathbf{q}(t)$. To demonstrate the influence of the input τ on the tracking error, the second derivative of e is calculated as

$$\ddot{\mathbf{e}} = \ddot{\mathbf{q}}_d(s(t)) - \ddot{\mathbf{q}}(t) \qquad (35)$$

Solving $\ddot{\mathbf{q}}$ from the equations of motion (1) and substituting into above equation yields

$$\ddot{\mathrm{e}} = \ddot{\mathrm{q}}_{\mathrm{d}}(\mathrm{s}(\mathrm{t})) + \mathrm{M}^{-1}(\mathrm{q})[\mathrm{C}(\mathrm{q},\dot{\mathrm{q}})\dot{\mathrm{q}} + \mathrm{g}(\mathrm{q}) - \mathrm{B}\tau] \quad (36)$$

Now, a PD controller is considered for the closed loop system such that the error dynamics is given as

$$\ddot{\mathbf{e}} = -\mathbf{K}_v\dot{\mathbf{e}} - \mathbf{K}_p\mathbf{e} \qquad (37)$$

Where $\mathbf{K}_p$ and $\mathbf{K}_v$ are positive diagonal matrices. Therefore, the following equation can be obtained from (36)

$$\mathrm{B}\tau = \mathrm{M}(\mathrm{q})\left[\ddot{\mathrm{q}}_{\mathrm{d}} + \mathrm{K}_{\mathrm{v}}\dot{\mathrm{e}} + \mathrm{K}_{\mathrm{p}}\mathrm{e}\right] + \mathrm{C}(\mathrm{q},\dot{\mathrm{q}})\dot{\mathrm{q}} + \mathrm{g}(\mathrm{q}) \quad (38)$$

On the other hand, using chain rule formula, $\ddot{\mathbf{q}}_d(s(t))$ are given as

$$\ddot{\mathbf{q}}_d = \mathbf{q}''_d(\mathrm{s})\dot{\mathrm{s}}^2 + \mathbf{q}'_d(\mathrm{s})\ddot{\mathrm{s}} \qquad (39)$$

By substituting (39) into (38) and using the matrixes $\mathrm{B}^{\perp}$ and B+, the control law τ and the second derivative of the time-scale parameter $\ddot{\mathrm{s}}$ are obtained from (38)

$$\begin{bmatrix}\tau\\ \ddot{s}\end{bmatrix} = \begin{bmatrix} I_{4\times4} & -\bar{\bar{M}}q_d' \\ 0_{1\times4} & \bar{M}q_d' \end{bmatrix}^{-1} \left[\begin{bmatrix}\bar{\bar{M}}(q)\\ \bar{M}(q)\end{bmatrix} \left(q_d'' \dot{s}^2 + K_v \dot{e} + K_p e\right) + \begin{bmatrix}\bar{\bar{C}}(q,\dot{q})\\ \bar{C}(q,\dot{q})\end{bmatrix}\dot{q} + \begin{bmatrix}\bar{\bar{g}}(q)\\ \bar{g}(q)\end{bmatrix}\right] \quad (40)$$

The second time derivative of $\mathbf{s}(t)$ determined from (40) is used as a supplementary input. Hence, the number of inputs are equal the number of outputs. Thereby we solve the underactuation problem. The values of matrices Kp and Kv are chosen to asymptotically track the desired trajectories at finite-time. Note that the control law (40) is a time-invariant controller and thus the closed-loop system is an autonomous system.

As obvious from (40), there is a singularity in the control law when $\bar{M}q_d' = 0$. In the neighborhood of desired motion this singularity is avoided since the condition (14) as forward motion constraint is satisfied during the desired trajectories. Therefore, the control law (40) is useful for one degree of underactuation in system.

5. Simulations

The geometric and inertia parameters of each link of biped are given in Table 1. Desired trajectories in joints space are determined by optimization of the mechanical work subjected to physical constraints and stability conditions described in Section 3. Here, we design an optimized trajectory for the biped robot walking with step length 0.35(m) and use the values described in Table 2 for the stable gait planning. Also, the desired posture of the torso is chosen upright.

Table 1- Geometric and inertia parameters of biped robot

Link	Torso	Thigh	Shank
Length (m)	0.75	0.40	0.50
Mass (kg)	9	2	1
Moment of Inertia (kgm^2)	0.422	0.027	0.02

Table 2- Utilized parameters to solve inverse kinematic equations

s	$x_{O4}(m)$	$y_{O4}(m)$	$x_H(m)$	$y_H(m)$
0.	0	0.05	0	0.87
1	0.35	0	0.17	0.86

After we obtain the stable reference motion from optimization process described in Section 3, we implement the control law (40) in order to track this stable motion during the single support phase. The gain matrices of the control law have been tuned such that the controller can follow trajectories before the heel of the swing leg hits on the ground at the first gait. Here, the diagonal values of $\mathbf{K}_v$ and $\mathbf{K}_p$ are chosen 37.5 and 350, respectively. The robot motion starts from the beginning of the single support phase by initial states restricted to the domain of Poincaré map (31).

The simulation data presented in figures 2–7 show efficiency of the method proposed in this paper. Here, the angle of the right and left legs shown in Fig. 1 are depicted as $q_{1R} = \theta_1$, $q_{2R} = \theta_2$, $q_{1L} = \sum_{i=1}^{4}\theta_i - \pi$, $q_{2L} = 2\pi - \theta_4$, respectively, and deviation of the torso from upright position is given as $\alpha = \theta_1 + \theta_2 + \theta_5 - 2\pi$, where θ_i, $1 \le i \le 5$ are as defined in Fig. 1.

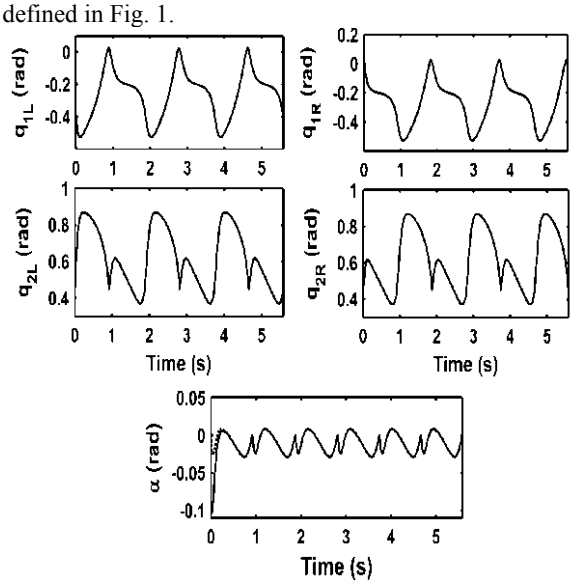

Fig.2: Tracking of the joint trajectories during three cycles, desired: dashed line and actual: solid line

Figure 2 shows efficiency of the proposed controller during three cycles to follow time-scale trajectories obtained from optimization process. In order to study asymptotically stable motion, the values of ζ_0 in gait K+1versus gait k is presented in Fig. 3. It is clear that ζ_0 converges to a unique value at cyclic value($\zeta_{0c} = -8.01$) after four gaits approximately as opposed to previous works that take at least 10-20 gaits[17].Figure 4 shows the evaluation of phase portrait of the torso, in where the convergence to the periodic orbit is clear. The joint torques of the right knee, left knee, hip and torso are provided in Fig. 5. It shows that the actuators create the feasible torques during motion. The ground reaction forces are shown in Fig. 6. The robot will not slip for a coefficient of friction greater than 0.5. The vertical force during the single support phase is close to the weight of the robot (from Table 1, its mass is 15kg). Snapshots of animation of the biped during one cycle are also displayed in Fig.7.

6. Demonstration of Robust Walking

In order to show robustness of the procedure described in this paper, we simulate the biped motion when it walks on the uneven surface. To this end, we assume the robot is walking on the level ground and suddenly the height of surface changes to an unexpected stair.

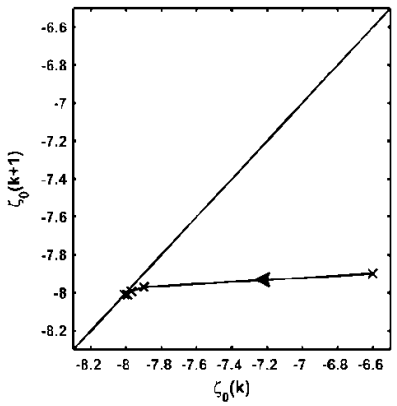

Fig. 3: The value of ζ_0 at step k+1 versus its value at step k which intersects with identity map in ζ_{0c}.

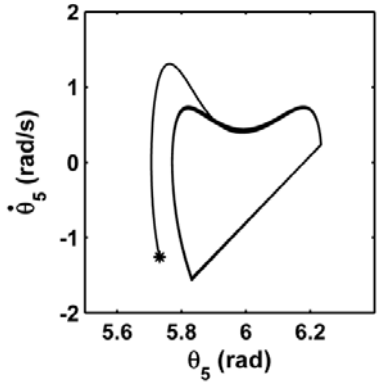

Fig. 4: Phase portrait of torso during motion

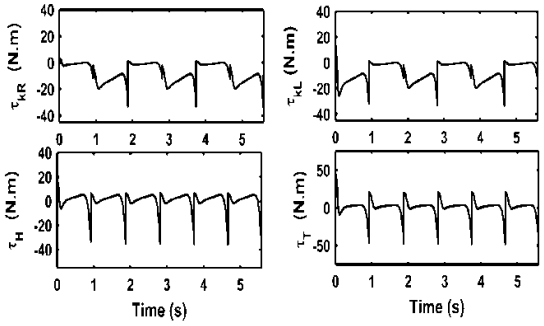

Fig. 5: Joint torques at hip and knee joints

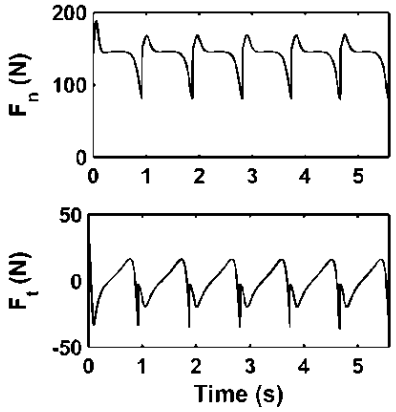

Fig. 6: Reaction forces during three cycles

Consider the biped robot has a stable walk during the first gait. In the second gait, the heel of the swing leg hits on the unexpected stair with height 20 mm. Note that this value is comparable with the nearly 50 mm of maximum height of the end of swing leg during motion. Figure 8 shows the phase portrait of the torso. Figure 9 displays the Poincaré map ζ_0 for third gait and after it.

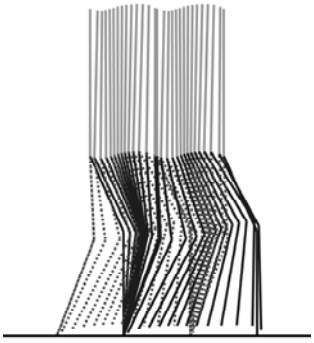

Fig. 7: Snapshots of animation of the biped taking one step from left to right.

It is obvious that ζ_0 converges to cyclic value after five gaits. These results show that the biped follows the prescribed cyclic motion after encountered with unexpected stair.

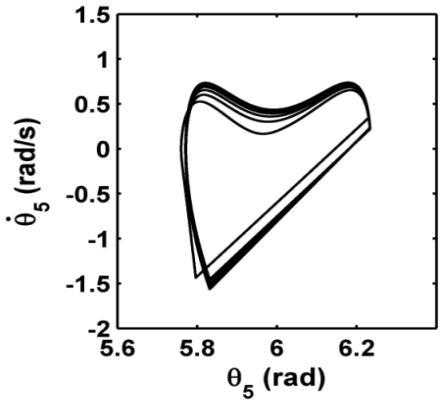

Fig. 8: Phase portrait of torso during motion in walking on the uneven surface.

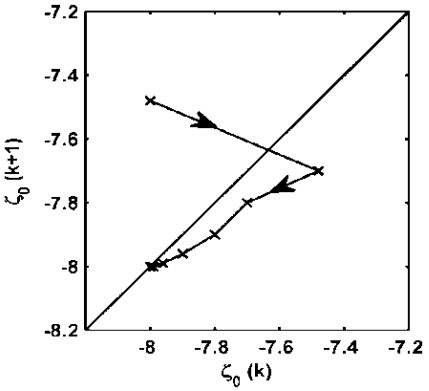

Fig. 9: Value of ζ_0 at step k+1 versus its value at step k which intersects with identity map in ζ_{0c} in walking on the uneven surface.

7. Elastic Contact Model

In previous simulations, it is assumed that the contact between the leg and the ground is rigid. While in the actual applications, this contact may not be rigid. This section presents the case where the biped robot has a elastic contact model and thus the dynamics model of the system at hand also incorporates the normal force on the stance leg due to a compliant contact with ground and the tangential force due to dynamic friction [22].

In this case, the biped robot has 7-DOF and the generalized coordinates are defined as $\mathbf{q}_f = [x_{O1}, y_{O1}, \theta_1, \theta_2, \theta_3, \theta_4, \theta_5]^T$. Based on these coordinates, the dynamic model is given as follows with a computation of the reaction forces acting on the end of the stance leg

$$\mathbf{M}_f(\mathbf{q}_f)\ddot{\mathbf{q}}_f + \mathbf{C}_f(\mathbf{q}_f, \dot{\mathbf{q}}_f)\dot{\mathbf{q}}_f + \mathbf{g}_f(\mathbf{q}_f) = \mathbf{B}_f\boldsymbol{\tau} + \mathbf{J}^T(\mathbf{q}_f)\mathbf{F} \quad (41)$$

Here, $\mathbf{M}_f(\mathbf{q}_f) \in R^{7\times7}$, $\mathbf{C}_f(\mathbf{q}_f, \dot{\mathbf{q}}_f) \in R^{7\times7}$, $\mathbf{g}_f(\mathbf{q}_f) \in R^7$, and $\mathbf{B}_f \in R^{7\times4}$. Also, $\mathbf{J}^T(\mathbf{q}_f)$ is the Jacobian matrix of the end of stance leg and $\mathbf{F}$ is the reaction forces acting on the end of stance leg given by

$$F_n = \begin{cases} k_v |y_{O_1}|^n - \delta_v |y_{O_1}|^n \dot{y}_{O_1} & y_{O_1} < 0 \\ 0 & y_{O_1} \geq 0 \end{cases}$$

$$F_t = (\alpha_1 \rho + \alpha_2 \dot{\rho} + \alpha_3 \dot{x}_{O_1}) F_n \quad (42)$$

$$\dot{\rho} = \dot{x}_{O_1} - \frac{\alpha_1}{\beta} |\dot{x}_{O_1}| \rho$$

The model of the normal force can be viewed as a nonlinear vertical spring-damper in terms of penetration of heel into ground y_{O_1}. The stiffness of the spring and the damping coefficient are denoted as k_v and δ_v, respectively. Also, n is a coefficient characterizing the form of the surfaces in contact. For this biped with point feet, it is assumed that a sphere at heel is in contact with a planar surface. Hence, the value of n is 3/2 for this contact [23].

The tangential force is obtained by using LuGre friction model [22]. In this model, it is assumed the interface of contacting surfaces is a contact between bristles. The bristle dynamics is modeled by horizontal spring and damper. Here, the average deflection of elastic bristles is denoted as ρ and its derivative is used as the internal state of the friction model. α_1 , α_2, α_3 and β are constants for this friction model.

Now, we implement the control law (40), which is derived by assumption of rigid contact model, into the biped model presented in (41) with the forces computed in (42).

The numerical values used in the simulation, given in Table 3, were adjusted for a nominal penetration of approximately 3 (mm) and to avoid rebound of the leg during the stance phase.

The simulation results are shown in figures 10-12. Figure 10 is depicted the joint trajectories and the amount of penetration. The phase portrait of torso is showed in Fig. 11 in which the convergence to limit cycle is clear even with elastic contact model. Also, the evolution of the angles is quite close to what was predicted with the rigid contact model (see figure 2). The reaction forces for two cases, i.e., rigid and elastic contact models are compared in Fig. 12. In order to compare these forces, we consider the same initial conditions and zero initial state errors at start of single support phase for both cases and then the control law (40) is used for them. Since a portion of energy is lost during penetration, the velocity of motion with elastic contact is less than rigid contact, as shown in Fig. 12. These results show the biped robot can follow a cyclic motion even with an elastic contact model.

Table 3. Elastic contact model parameters

Parameter	k_v(N /m$^{3/2}$)	δ_v(N.s /m$^{5/2}$)	α_1(m^{-1})	α_2(s /m)	α_3(s /m)	β
Value	8.9 $\times 10^5$	4.6 $\times 10^3$	260	0.6	0.018	0.5

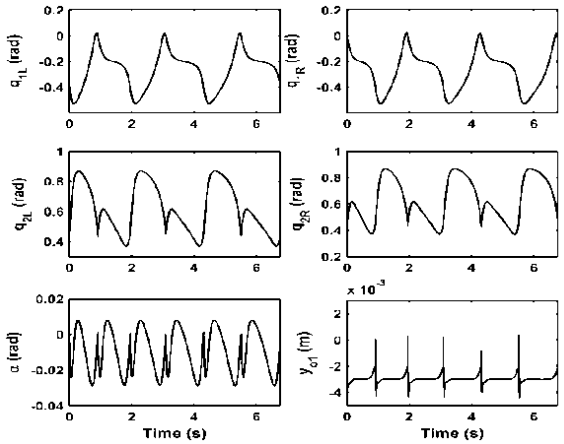

Fig. 10: Evaluation of the joint trajectories and penetration with flexible contact model

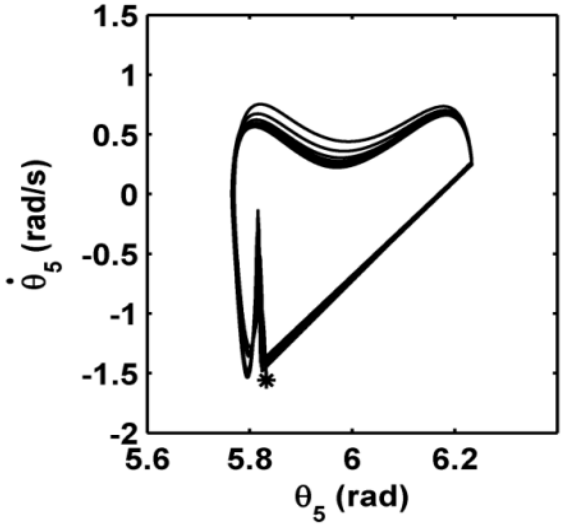

Fig. 11: Phase portrait of torso in walking with flexible contact model

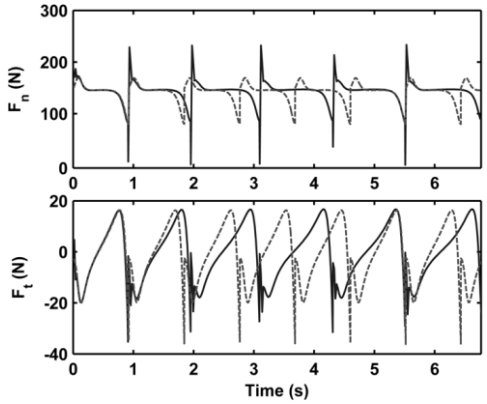

Fig. 12: Comparison of reaction forces for two case with rigid contact model (dashed line) and flexible contact model (solid line)

8. Conclusions

An optimization process and a time-invariant feedback control strategy have been developed in order to obtain a stable motion for a five-link biped walker. Using the Poincaré map associated with the unactuated dynamics, an explicit criterion for the existence of periodic orbits and characterization of their stability properties were derived. The simulation results show that the biped follows the prescribed cyclic motion after a few gaits even since encountered with unexpected stair. Also, the results showed the biped can follow a cyclic motion when the biped is walking on the compliant surface.

References

[1] J. Kanniah and Z. N. Lwin, ZMP compliant gait generation strategies for seven-mass biped robots, International Journal of Humanoid Robotics, 5(4) (2008) 609-637.

[2] S.A.A. Moosavian, M. Alghooneh, A. Takhmar, Stable trajectory planning, dynamics modeling and fuzzy regulated sliding mode control of a biped robot, IEEE-RAS International Conference on Humanoid Robots, Pittsburgh, USA, 2007, pp. 471-476.

[3] M. Vukobratovic, B. Borovac, Zero-moment point – thirty five years of its life, International Journal of Humanoid Robotics, 1(1) (2004) 157–173.

[4] T. McGeer, Passive dynamic walking, International Journal of Robotics Research, 9(2) (1990) 62–82.

[5] E. Borzova, Y. Hurmuzlu, Passively walking five-link robot, Automatica, 40 (2004) 621-629.

[6] A. Formal'sky, Y. Aoustin, On the stabilization of a biped vertical posture in single support using internal torques, Robotica, 23(1) (2005) 65-74.

[7] C. Chevallereau, A. Formal'sky, D. Djoudi, Tracking of a joint path for the walking of an underactuated biped, Robotica, 22(1) (2004) 15-28.

[8] C. Chevallereau, E. R. Westervelt, J. W. Grizzle, Asymptotically stable running for a five-link four-actuator planar bipedal robot, International Journal of Robotics Research, 24(6) (2005) 431-464.

[9] Y. Aoustin, A. Formal'sky, Control design for a biped: Reference trajectory based on driven angles as function of the undriven angle, Journal of Computer and System Sciences International, 42(4) (2003) 159-176.

[10] S. K. Agrawal, A. Fattah, Motion control of a novel planar biped with nearly linear dynamics, IEEE/ASME Transactions on Mechatronics, 11(2) (2006) 162-168.

[11] A. Chemori and A. Loria, Control of a planar underactuated biped on a complete walking cycle, IEEE Transactions on Automatic Control, 49 (2004) 838–843.

[12] V. Sangwan, S. K. Agrawal, Differentially flat design of bipeds ensuring limit-cycles, IEEE International Conference on Robotics and Automation, (Roma, Italy, 2007), pp. 3589-3590.

[13] T. Geng, B. Porr, F. Wörgötter, Fast biped walking with a sensor-driven neural controller and real-time online learning, International Journal of Robotics Research, 25(3) (2006) 243-259.

[14] J. W. Grizzle, G. Abba, F. Plestan, Asymptotically stable walking for biped robots: analysis via systems with impulse effects, IEEE Transaction on Automatic Control, 46 (1) (2001) 51-64.

[15] L. Cambrini, C. Chevallereau, C. H. Moog, R. Stojic, Stable trajectory tracking for biped robots, Proceedings of IEEE Conference Decision and Control, (Orlando Florida, 2001), pp. 4815-4820.

[16] E. R. Westervelt, J. W. Grizzle, D. E. Koditschek, Hybrid zero dynamics of planar biped walkers, IEEE Transactions on Automatic Control, 48(1) (2003) 42-56.

[17] E. R. Westervelt, G. Buche, J.W. Grizzle, Experimental Validation of a Framework for the Design of Controllers that Induce Stable Walking in Planar Bipeds, International Journal of Robotics Research, 23(6) (2004) 559-582.

[18] M. Nikkhah, H. Ashrafiuon, and F. Fahimi, Robust control of underactuated bipeds using sliding modes, Robotica, 25 (2007) 367–374.

[19] A. D. Kuo, Stabilization of lateral motion in passive dynamic walking, International Journal of Robotics Research, 18(9) (1999) 917–930.

[20] Y. Hurmuzlu, T. H. Chang, Rigid body collisions of a special class of planar kinematic chains, IEEE Transactions on Systems, Man, and Cybernetics, 22(5) (1992) 964-971.

[21] A. Goswami , B. Espiau , A. Keramane , Limit cycles and their stability in a passive bipedal gait, Proceedings of the 1996 IEEE International Conference on Robotics and Automation (Minneapolis, Minnesota, 1996), pp. 246-251.

[22] C. Canudas, H. Olsson, K. J. Astrom, P. Lischinsky, A new-model for control of systems with friction, IEEE Transactions on Automatic Control, 40(3) (1995) 419-125.

[23] W. D. Marhefka, D. E. Orin, A compliant contact model with nonlinear damping for simulation of robotic systems, IEEE Trans. Syst., Man and Cybernetics. part A: System and Humans, 29(6) (1999).

Biography of Authors

Reza Dehghani has received M.Sc. degree in mechanical engineering from Isfahan University of Technology in 2004 and completed his Ph.D. degree in mechanical engineering at the same institute in 2010. His research interests include humanoid robots, dynamics and control of robotics manipulators and biped robots, and nonlinear control systems.

Abbas Fattah has completed his Ph.D. degree in mechanical engineering from McGill University in 1995. He has been in Department of Mechanical Engineering at Isfahan University of Technology as a faculty and with Department of Mech. Engineering at University of Delaware as a visiting professor and research scholar. His research activities are now mainly on dynamics, design, and control of special mechanical systems such as rehabilitation robots, bipeds, cable-suspended robots, and parallel mechanisms. He has published several patents and more than 70 articles in international journals and conferences. The results of his research have novelty in the field of robotics and mechanical systems.